COBEM 2021 26th International Congress of Mechanical Engineering
ABCM Associação Brasileira de Engenharia e Ciências Mecânicas
November 22-26, 2021, Virtual Congress, Brazil

COB-2021-1827
INTERACTION BETWEEN NATURAL CONVECTION AND SURFACE RADIATION IN A LOW ASPECT RATIO RECTANGULAR ENCLOSURE WITH DIFFERENT WALL EMISSIVITIES

Leandro Manes
Eduardo Larsen Güths
Saulo Güths
Department of Mechanical Engineering, Federal University of Santa Catarina, PO Box 476, Postal Code 88040-970, Florianópolis, SC, Brazil.

Ldmnes@gmail.com
e.l.guths@gmail.com
saulo.guths@lmpt.ufsc

Abstract. *The interaction of coupled surface radiation and laminar natural convection in a vertical cavity heated from the side and with horizontal adiabatic walls is analyzed numerically in this study. The numerical calculations were performed using the numerical software ANSYS CFX. Air flow in the cavity is governed by the Navier-Stokes equations under the Boussinesq assumption. Also, it is assumed that air is incompressible and radiatively non-participating. The study covers Rayleigh Numbers of* 10^3 *to* 10^6 *and aspect ratios of 1 to 10. The emissivity of the walls varies from 0 to 1 and the values differ or are the same for each wall depending on the case. The temperature of the cold wall was fixed at 288.5 K and that of the hot wall at 298.5. The results of this study show that the radiation heat transfer influences the overall heat transfer even for cavities with low emissivity. They also indicate that the total Nusselt number decreases with increasing aspect ratio. In the cases where the walls have different emissivity values it is clear that the influence of the horizontal wall emissivity was small compared to that of the vertical wall emissivity. The separate analysis of cold and hot wall surface emissivity shows that the increase in* Nu_r *with an increase in* ε_h *is slightly higher than that with the increase in* ε_c*. Although the effect of* ε_h *is greater, is it clear that* Nu_r *is strongly dependent on both* ε_h *and* ε_c*. Thus, in cases where the goal is to reduce the heat transfer, decreasing the emissivity of only one of the walls is effective.*

Keywords: *Natural Convection, Radiative Heat Transfer, Convection Heat Transfer*

1. INTRODUCTION

The prediction of heat transfer in differentially heated vertical cavities filled with air is important for a number of engineering applications, including heating and cooling in buildings, heat transfer through double glazed windows, solar calorimeters, and many others.

Most of the phenomena related to a temperature difference involve more than one mechanism of heat transfer. Nevertheless, in recent decades, applying simplified analysis (without taking the surface radiation into account), many researchers have been studying free convection inside cavities and have been publishing experimental and numerical results about it. In the 1980s, De Vahls Davis [0] solved the problem of natural convection in a square cavity and his results are still accepted worldwide. In his solution, emphasis was given to the average convection Nusselt number ($\overline{Nu_c}$) throughout the cavity as a function of the Rayleigh number and the correlation between them can be expressed as: $(\overline{Nu_c}) = f(Ra, Pr)$. Davis considered a two-dimensional fluid flow with Prandt = 0.71 inside a square cavity of side L. The working fluid was air and the Boussinesq approximation was used. Davis also considered velocity components to be zero at the boundaries. The horizontal walls are insulated, and the vertical sides are at temperatures T_h and T_c, where $T_h > T_c$. The solution of this problem was limited to a Rayleigh number of 10^6.

The literature review revealed that several studies have been carried out on natural convection heat transfer, for a broad range of Ra and A values. However, the number of studies focused on coupled convection and radiation heat exchange, particularly for low A and with different ε_w, is low. It is known that in several applications involving heat transfer there are surfaces made of different materials, some of them painted, for which the heat transfer can be considerably increased or decreased simply by painting certain surfaces with a highly absorptive or reflective paints. Therefore, the aim of this study was to investigate the impact of using different combinations of A, ε_w and other variables to better understand the real systems found in many engineering fields.

2. NUMERICAL MODELING AND MATHEMATICAL FORMULATION

2.1 Software used

The numerical simulations were performed using the numerical software ANSYS CFX, a computational fluid dynamics (CFD) software program. Different geometries were designed using the design modeling tool of ANSYS 14 Workbench and the bodies were then imported with a meshing tool to generate an appropriate mesh. After meshing, the boundary conditions were specified, and the simulation solved. CFX Post provided the results. The set of equations used in CFX, which describes the processes of momentum, heat and mass transfer are described in section 2.3. CFX uses the finite volume technique to solve these equations.

2.2 Physical model and assumptions

Figure 1 shows the basic aspects of the model, which consists of a two-dimensional cavity with side L and height H. The horizontal walls are considered adiabatic. The left and right sides are maintained at temperatures of T_c =288.5 K and T_h=298.5 K, respectively. The walls are considered gray-diffuse with emissivities of $\varepsilon_t, \varepsilon_b, \varepsilon_h, \varepsilon_c$. The air is assumed to be incompressible and radiatively non-participating. Gravity acceleration acts in a negative v-direction; the fluid was approximated (Boussinesq-approximation) and its properties were taken from the Engineering Equation Software (EES) library at the average temperature ($\frac{T_c+T_h}{2}$). The aspect ratio is defined as $\left(\frac{H}{L}\right)$

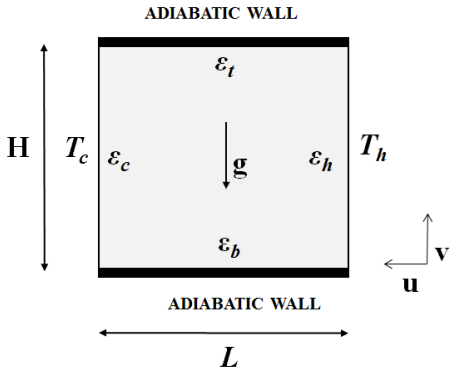

Figure 1: Basic aspects of the model.

2.3 Mathematical formulation

2.3.1 Radiation

There are several methods described in the literature to solve radiation heat transfer. ANSYS CFX provides four of them [0]. The P1 and Rosseland models are recommended for solving problems where the material is optically dense and actively participates in the heat transfer process. In situations where the material is considered transparent to radiation at the wavelengths at which most of the heat transfer occurs, the Monte Carlo model is a very good option; however, it requires high computational power. The discrete transfer model (DTRM) has also been used to predict heat transfer in thin optical materials (e.g. air and other gaseous media). After running many tests for a specific set of boundary conditions the outcomes of the Monte Carlo model and the DTRM were the same. Since the latter is faster, this method was used to model radiation heat transfer in the study reported herein. Furthermore, as noted in the literature review, Shati [0] also used this method and obtained good results.

DTRM is based on tracing the domain with multiple rays leaving the boundary surfaces. The ray tracing technique used in the DTRM can provide a prediction of the radiation heat transfer between surfaces without explicit view factor calculations [0]. The accuracy of the model is dependent on the number of rays traced and the computational grid. By assuming that the radiation intensity, *I*, is independent of the direction and wavelength, the equation for the change in the radiant intensity, *dI*, along a path, ds, can be written as $\frac{dI}{ds} + Ia = \frac{\sigma a T^4}{\pi}$, where (a) is the absorption coefficient, T is the local air temperature, and σ is the Stefan-Boltzmann constant.

Equation 2.5 is then integrated along a series of rays emanating from boundary faces so that the radiation intensity is $I(s) = \frac{\sigma T^4}{\pi}\ (1 - e^{-as}) + I_0 e^{-as}$, where I_0 is the radiant intensity at the start of the incremental path, which is determined by the appropriate boundary conditions.

At each radiation face, rays are calculated for different values of the polar (θ) and azimuthal (Φ), where, $0 < \theta < \frac{\pi}{2}$ and $0 < \Phi < 2\pi$. Each ray is then traced to determine the control volumes it intercepts as well as its length within each control volume. Thus, no view factor is required. This information is stored in a file and it must be input before the flow calculations start. For the ray tracing method, the incident radiation heat flux (q_{in}) on a wall surface is $q_{in} = \int_{\vec{s}.\vec{n}>0} I_{in}\vec{s}.\vec{n}\, d\Omega$, where I_{in} is the intensity of the incoming ray, $\vec{s}$ is the ray direction vector, $\vec{n}$ is the normal pointing out of the domain and Ω is the hemispherical solid angle. Considering longwave radiation, the net radiation heat flux from the surface (q_{out}) is the sum of the reflected portion of q_{in} and the emissive power of the surface, where T_w is the surface temperature and ε_w is the wall emissivity $q_{out} = (1-\varepsilon_w)q_{in} + \varepsilon_w \sigma T_w^4$

ANSYS CFX also provides the option to use the surface to surface (S2S) method for non-participating media, but in contrast to the traditional S2S method there is no view factor calculation. In this case the approach is the same as that of the DTRM method, however, a is set to zero. Therefore, there is no interaction between the fluid and the ray and, consequently, $\frac{dI}{ds} = 0$. In other words, with this option the volumetric emission, absorption and scattering are ignored, regardless of the specified material properties. This makes the simulation run much faster. This strategy is well accepted in the academic field for thin optical materials such as air and other gaseous media. After running tests it was found that the predictions using DTRM with and without the S2S mode activated were similar, but with S2S the procedure was faster. Therefore, the S2S method, using the principles of DTRM to eliminate the view factor calculation, provided the radiation heat exchange. Clearly, the use of S2S with the view factor calculation would be faster, but unfortunately CFX does not provide this option.

2.3.1 Nusselt Calculation

To determine the steady-state heat transfer characteristics at both vertical walls, contributions of both convection and radiation should be taken into consideration. In this study the average radiative, convective, and total Nusselt numbers are introduced respectively as $\overline{Nu_r} = \frac{\overline{q_r}L}{k_f(T_h - T_c)}$, $Nu_c = \frac{\overline{q_c}L}{k_f(T_h - T_c)}$, $Nu_t = \overline{Nu_c} + \overline{Nu_r}$, where $\overline{q_r}$ and $\overline{q_c}$ are the average radiation and convection heat flux of both walls $(\overline{q_h} + \overline{q_c})/2$ and k_f is the air conductivity.

3. VALIDATION OF RESULTS

3.1 Assumptions to achieve reliable results

Verification and validation (V&V) are the primary means to achieve accuracy and reliability in CFD simulations. Although there is disagreement among researchers in this area regarding the most appropriate procedures for the verification and validation of CFD simulations, the importance of quantifying the levels of uncertainty and error is broadly accepted. One indication of the non-convergence of the solution to steady state is large residual values. According to Zitzmann [0], a root mean square (RMS) residual in the range of 10^{-4} to 10^{-5} is acceptable in most cases. In the present study, the RMS residual was set at 10^{-6}, in order to achieve high-accuracy results. Low global imbalance is also very important and this parameter was set at < 0.01%.

To reduce the computational effort, a grid independence study was carried out. To avoid excessive temperature and velocity steps imposed by the boundary conditions. Shati [0], for instance, generated the non-uniform grid using an expression that allowed them to obtain a finer mesh close to the boundaries. CFX also has this capability.

Grid independence was tested considering a square cavity with $\mathrm{Ra} = 10^6$ and $\varepsilon_w = 1$. The numbers of grids as well as the bias factor were increased progressively. Figures 3a and 3b show the deviations in $\overline{Nu_r}$ and $\overline{Nu_c}$, respectively. The deviation is obtained from the ratio of the average Nusselt number in each grid number to the last Nusselt number (as a percentage). The deviation is plotted versus grid numbers for bias factors of 1 to 9.

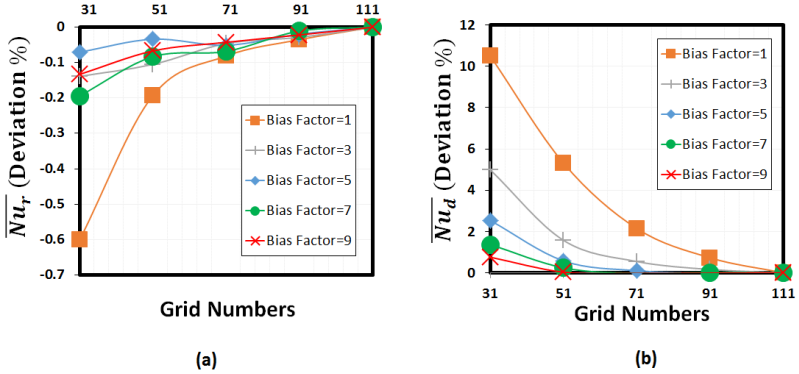

Figure 2: Grid convergence study.

As observed in Figure 2, $\overline{Nu_r}$ is almost insensitive to the grid number varying less than 0.6%. while the opposite scenario is seen for $\overline{Nu_c}$. Similarly to the findings of other authors [0,0], it was also verified that a higher grid concentration near the walls improves the natural convection convergence. In Figure 3 it is clear that an increase in the bias factor affected significantly the results for the same number of elements. Therefore, it allows convergence to be achieved with a lower number of elements, saving on computational power. After also analyzing the simulation results for other Ra values, the combination of a bias factor of 7 and grid number of 71 was choosen for square cavities. For higher aspect ratios, a higher number of elements was used in the vertical direction. To find this number, grid convergence was tested for $A = 10$. Similarly, to [0], it was found that using 3 times more elements in the vertical direction is sufficient to achieve accurate results. For other aspect ratios between 1 and 10 the grid number was calculated using a linear approach. For instance, when $A = 4$, the number of elements in the horizontal direction was 71 and in the vertical direction it was $(1 + (A/10) * 2) * 71 = 127.8$ or in this case 128. The bias factor remained at 7 for all A values.

3.2 Model Validation

To validate the convective part of the simulation, a square cavity with $T_h = 298.5\,K$ and $T_c = 288.5\,K$ was simulated. Since this is a pure convection case, $\varepsilon_w = 0$. Firstly, the results were compared with those of other studies available in literature focused only on convection (references [1,7,8]). shows the excellent agreement between the experimental and simulated data for $\overline{Nu_c}$, which verifies the accuracy of ANSYS CFX and the approach used in the simulation. In the next step, in order to verify that the simulation performed well with the introduction of radiative analysis, the emissivity was changed to 1 and the results compared with those reported in references [0,0]. As can be seen in the Nusselt number with $\varepsilon = 1$ exhibited good agreement for Ra $= 10^3, 10^4$ and 10^5. However, for Ra $= 10^6$ there was a small deviation. On analyzing the results of all researchers included in Table 1, a deviation also occurred when $\varepsilon_w = 0$ in the convection component. The $\overline{Nu_c}$ values with $\varepsilon_w = 0$ of references [0,0] were higher than 9, while researchers who studied only convection heat transfer obtained values lower than 9. However, besides the difference observed for Ra $= 10^6$, the drop in $\overline{Nu_c}$ for Ra $= 10^6$ due to the introduction of radiation was similar (around 15%) for all three studies based on coupled models. It was thus concluded that the coupled model performs well.

Table 1 Convection verification - results and comparison using grid of 71x71 elements.

		$\varepsilon = 0$				$\varepsilon = 1$				Drop of $\overline{Nu_c}$ (%)
	Rayleigh	**10^3**	**10^4**	**10^5**	**10^6**	**10^3**	**10^4**	**10^5**	**10^6**	**10^6**
Pure convection	De Vahl Davis [0]	1.12	2.243	4.52	8.8	-	-	-	-	-
	D. C. Wan (DSC) [0]	1.073	2.155	4.352	8.632	-	-	-	-	-
	D. C. Wan (FEM) [0]	1.117	2.254	4.598	8.976	-	-	-	-	-
	Massarotti [0]	1.117	2.243	4.521	8.806	-	-	-	-	-
Convection + Radiation	**Present study**	**1.115**	**2.242**	**4.527**	**8.887**	**1.244**	**2.221**	**4.116**	**7.696**	**15.48**
	Bahlaoui [0]	1.118	2.257	4.627	9.475	1.250	2.242	4.192	8.100	16.98
	Akiyana [0]	1.125	2.250	4.625	9.375	1.250	2.250	4.250	8.125	15.38

For further comparison, the model results were compared with those obtained in studies carried out by Moutaouakil et al. [0] for A=10, $Ra = 3.93\,x\,10^5, 0 \leq \varepsilon_w \leq 1$, $T_h = 333\,K$, $T_c = 293\,K$. Figure 4 shows this comparison for laminar flow. The radiation heat transfer results were in very good agreement. However, there was a small deviation in the convection heat transfer since Moutaouakil et al. used a turbulence model instead of a laminar model. On adopting the same turbulence model in CFX the results matched very well. However, the laminar model was maintained since Ra $< 10^6$. Moutaouakil used the turbulence model because they studied larger aspect ratios $10 \leq A \leq 80$. Since this study is focused on $1 \leq A \leq 10$, the laminar model is an acceptable option.

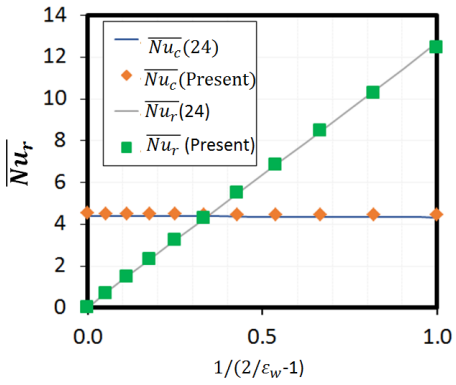

Figure 3: Comparison of Nusselt numbers obtained in this study with those reported in reference [0].

4. RESULTS AND DISCUSSION

4.1 Pure Convection Heat Transfer

Firstly, the effect of natural convection in an enclosure without surface thermal radiation was studied. Similarly to other researchers [0,0], it can be seen in Figure 4 that in general $\overline{Nu_c}$ decreases as A increases. Nevertheless, for Ra $= 10^3$ $\overline{Nu_c}$ is almost independent of A since there is a strong conductive regime for this Rayleigh number. As the Rayleigh number increases, the conductive component diminishes and $\overline{Nu_c}$ becomes more dependent on A.

The velocity and temperature profiles for the non-radiating case with Ra $= 10^5$ and $A = 1, 2, 6, 10$ are shown in Figure 5. In each case the fluid rises along the hot wall and falls along the cold wall, as expected.

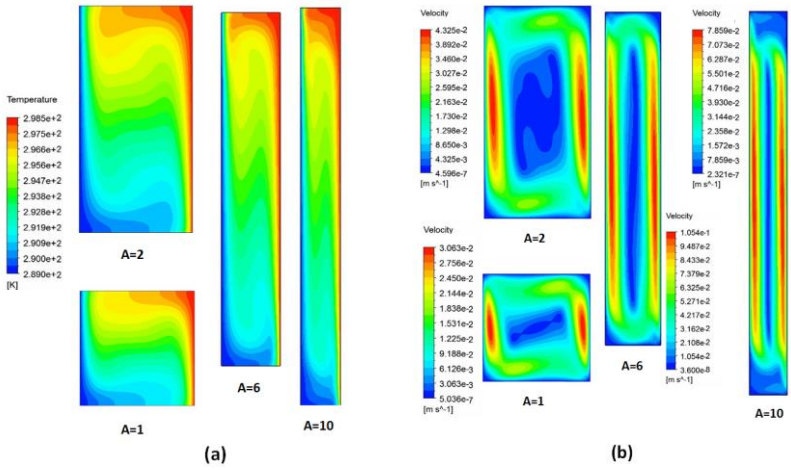

Figure 4: Temperature (a) and velocity (b) profiles for Ra=10^5 for several aspect ratio (A) values.

A visual comparison of the results for the four A values shown in Figure 4 indicates that the velocity and thermal boundary layers tend to become thicker as A increases. This hypothesis was confirmed by plotting the velocity and temperature profiles at the middle height. It is clear from Figure 6 that both the thermal and velocity boundary layers become thicker with increasing A values, which is one of the explanations for the drop in $\overline{Nu_c}$, since a thinner boundary layer improves the heat transfer and, consequently, $\overline{Nu_c}$ increases.

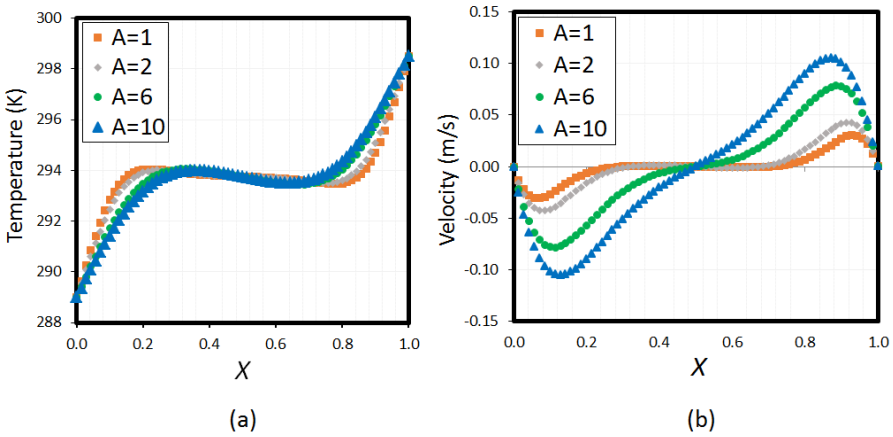

Figure 5: Temperature (a) and velocity (b) profiles at middle height (Y=0.5).

Using the same principle applied by other researchers, revealed in a review of the literature, six correlations were proposed (one for each A value) adopting the power-law correlation $(\overline{Nu_c}) = cRa^a$. These can be seen in Table 2 and are valid for $1 \leq A \leq 10$ and $10^3 \leq Ra \leq 10^6$. They were created by using a power fit to the points shown in **Erro! Fonte de referência não encontrada.**.

The largest absolute error of the 6 correlations was 6.87% which occurred for Ra= 10^3 and A=10. The average error of the correlations was lower than 2% for the proposed range. Interpolation can be used in the case of an A value which was not considered.

Table 2: Nu_c correlations for pure convection heat transfer.

Aspect Ratio	1	2	4	6	8	10
Correlation	$0.1381Ra^{0.3022}$	$0.1874Ra^{0.2719}$	$0.1841Ra^{0.2633}$	$0.176Ra^{0.2603}$	$0.1698Ra^{0.2583}$	$0.1661Ra^{0.2559}$

4.2 Coupled Convective and Radiative Heat Transfer

As seen in the previous section, variations in A and Ra have a strong influence on $\overline{Nu_c}$. Since the aim of this study was also to examine the influence of the emissivity, the radiation mode was turned on and the effects of A, Ra and ε_w on Nu_c and Nu_r analyzed. Figure 8 shows the interaction between convective and radiative heat transfer for $1 \leq A \leq 10$, $0.05 \leq \varepsilon_w \leq 1$ and $Ra = 10^3, 10^4, 10^5, 10^6$. The same emissivity distribution was set for all four walls. $\overline{Nu_r}$ as a function of a variation in ε_w is shown in Figure 6 column a (1-4) for different Ra and A values. As expected, an increase in the emissivity resulted in greater radiative heat exchange and, consequently, higher $\overline{Nu_r}$ values. It is interesting to note that here an increase in A leads to an increase in $\overline{Nu_r}$, while the opposite trend was found for $\overline{Nu_c}$ in the pure convection case described in the previous section.

On analyzing $\overline{Nu_c}$ in Figure 7 column b (1-4) and column c (1-4), the introduction of emissivity affected $\overline{Nu_c}$ as expected. Similarly, to the observations presented by Akiyama and Chong [0], there is a drop in $\overline{Nu_c}$ for $Ra = 10^5; 10^6$. On the other hand, for $Ra = 10^4$ there is almost no variation in $\overline{Nu_c}$ and for $Ra = 10^3$ $\overline{Nu_c}$ increases. Figure 8 column c (1-4) shows the deviation of $\overline{Nu_c}$ in percentage terms $(\overline{Nu_{c,d}}(\%))$ when compared to Nu_c for the pure convection case. Additionally, the $(\overline{Nu_{c,d}}(\%))$ value was lower for higher A values for the same emissivity. However, the drop in $\overline{Nu_c}$ was much lower than the increase in $\overline{Nu_r}$.

Figure 6 column d (1-4) shows the increase in $\overline{Nu_t}$ on taking ε_w into account. In general, this shows that the total Nusselt deviation $\overline{Nu_{t,d}}$ increases with increasing A and ε_w values. For instance, considering the combination of $\varepsilon_w = 1$, A=10, $Ra = 10^6$, $\overline{Nu_r}$ is around 350% higher than it would be if only convection was considered. This means that not taking radiation heat transfer into account would lead to large errors in the heat transfer prediction.

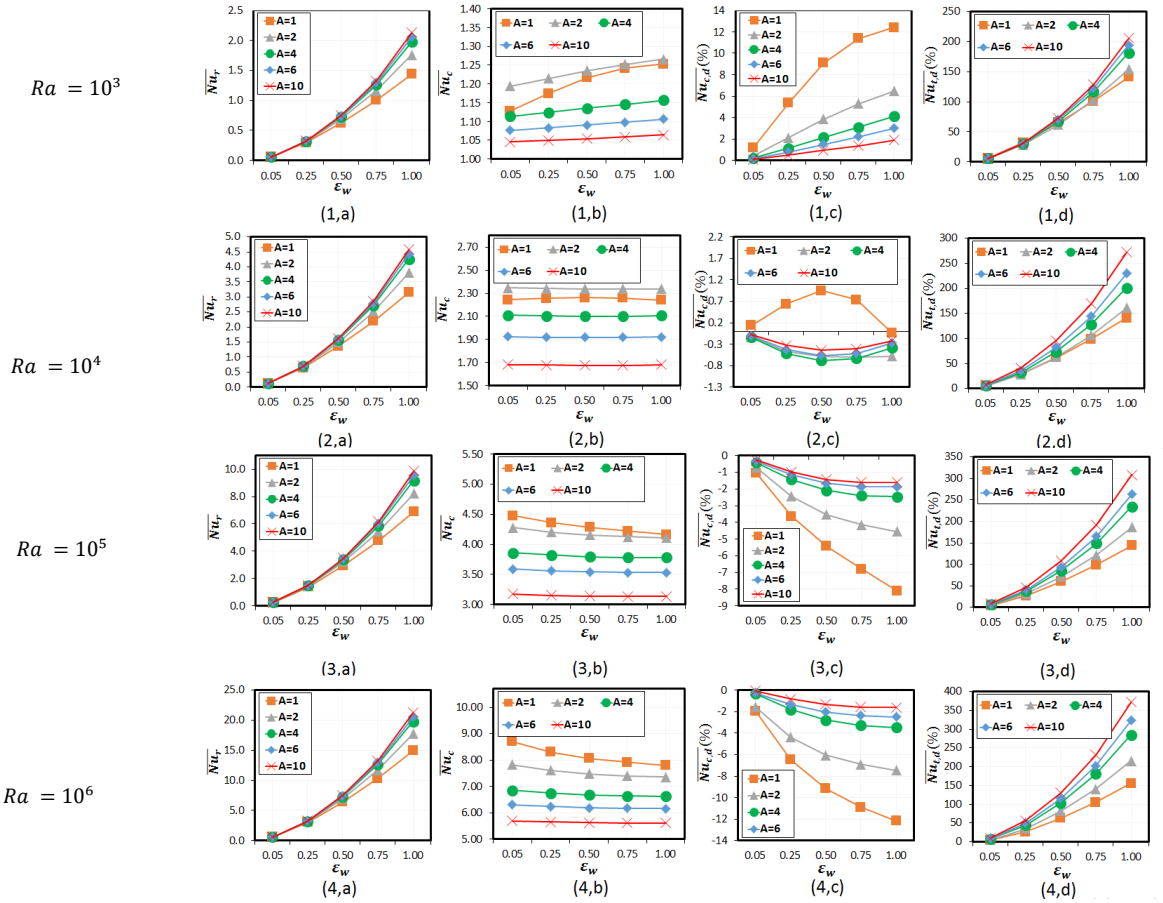

Figure 6: Influence of variations in the Ra, A and ε values (all walls with the same emissivity distribution).

To gain a better understanding in physical terms, 8 shows the temperature profiles for A=1, 2 and 6, and Ra=10^5, with and without radiation ($\varepsilon_w = 1$ and $\varepsilon_w = 0$, respectively). The effect of high emissivity of the walls is visible for all aspect ratios (A), especially close to the horizontal walls. The temperature of the convection plume rising at the hot wall decreased at the top in contrast to the case without radiation ($\varepsilon_w = 0$). The opposite occurs at the cold wall: the cold plume which is descending close to the cold wall increased in temperature in the case where emissivity was present.

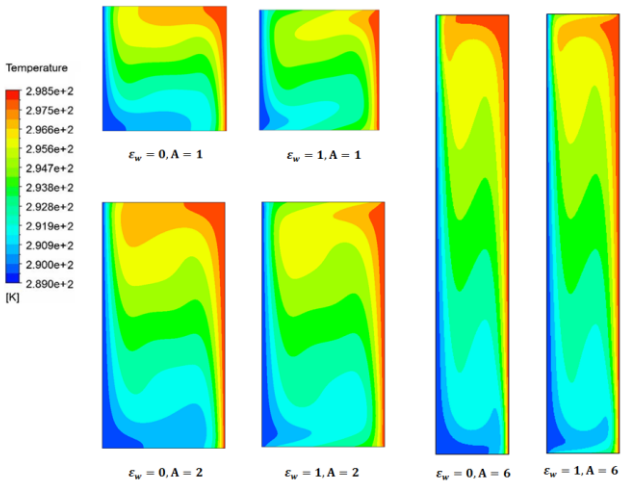

Figure 7: Temperature profiles for A=1, 2 and 6, Ra=10^5, with and without radiation ($\varepsilon_w = 1$ and $\varepsilon_w = 0$).

Seeking to explain the effect of the emissivity on the flow pattern, fluid temperature and velocity profiles at Y=0, Y=0.5 and Y=0.9, for the case A=1 and Ra=10^5, with and without radiation ($\varepsilon_w = 1$ and $\varepsilon_w = 0$) were plotted (Figure 7). As can be seen in the figure, the velocity profile (a) is only slightly modified by the radiation exchange. On the other

hand, the temperature profile (b) is strongly affected by the radiation heat exchange. On analyzing the top region (Y=0.9) of the cavity, a considerable reduction in the fluid temperature can be observed when there is heat transfer by radiation. At the bottom (Y=0.1) the phenomenon is the opposite, and in the middle (Y=0.5) there is no modification of the temperature profile.

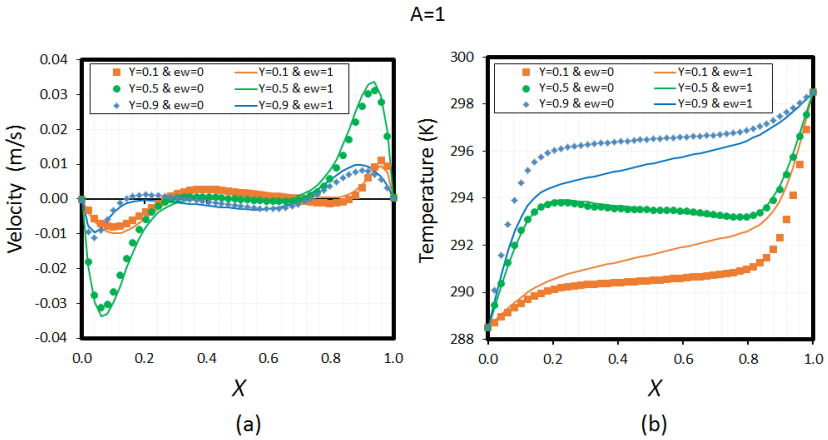

Figure 8: Fluid velocity (left), fluid temperature (right) and profiles for Y=0.1, Y=0.5 and Y=0.9. A=1 and Ra=10^5 with and without radiation ($\varepsilon_w = 1$ and $\varepsilon_w = 0$).

The fluid temperature profile at the hot wall shows an increase in the gradient close to the top surface, as shown in figure 9a (X=1.0, Y=0.9), when the radiation is considered, which will lead to an increase in the Nu_c value in this region. Nevertheless, in the bottom region of the same surface (X=1.0, Y=0.1) the effect is the opposite - the temperature gradient decreases when radiation heat exchange is considered and thus Nu_c for $\varepsilon_w = 0$ will be higher. In order to better illustrate this, Figure 9 shows the local convective Nusselt numbers at X=0 and X=1, but here $\varepsilon_w = 0.05$ was simulated instead of $\varepsilon_w = 0$, as shown in Figure , to be consistent with Figure 6 (3,b). It can be observed that Nu_c increases at the top due to the larger temperature gradient for $\varepsilon_w = 1$, X=1 and Y~1 and decreases for $\varepsilon_w = 1$, X=1 and Y~0 due to a smaller temperature gradient, as mentioned above.

The phenomenon on the cold side is symmetrically similar and is also in agreement with the results shown in Figure . For instance, in Figure 7 at the top (Y=0.9 and X=0), the largest temperature gradient was for the case where $\varepsilon_w = 0$. As predicted, Figure 9 shows a higher Nu_c value for X=0 and Y~1 in the radiation-free case. The transformation from Nu_c to $\overline{Nu_c}$ can be carried out using integration. For instance, integrating at X=0 and X=1 from Y=0 with $\varepsilon_w = 0.05$ results in $\overline{Nu_c} = 4.48$ and integrating at X=0 and X=1 from Y=0 with $\varepsilon_w = 1$ results in $\overline{Nu_c} = 4.12$, which are the results given earlier in Figure 6 (3,b) for A=1. It is also interesting to note that the Nu_c value is higher close to the top at the cold wall and close to the bottom at the hot wall. Once again, this difference is caused by the large temperature gradient.

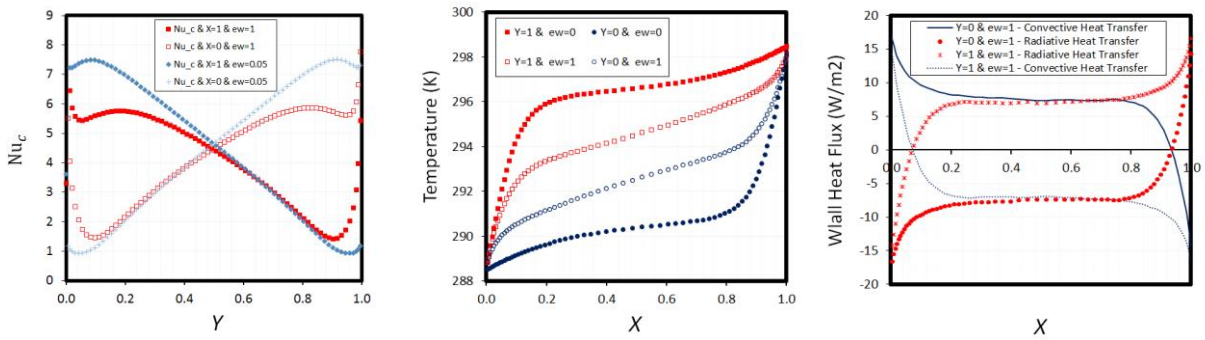

Figure 9: In the Left side Nu_c at the hot side (X=1) and cold side (X=0) and Ra=10^5 with high and low radiation levels ($\varepsilon_w = 1$ and $\varepsilon_w = 0.05$). In the middle Surface temperature at the top (Y=1) and the bottom (Y=0) for A=1 and Ra=10^5, with and without radiation ($\varepsilon_w = 1$ and $\varepsilon_w = 0$); at the right side, heat flux by convection and by radiation at the bottom (Y=0) and top (Y=1) surfaces in a square cavity with $\varepsilon_w = 1$.

4.3 Influence of different wall emissivities for cold and hot walls

The goal in this section is to analyze the effect of different wall emissivities on the average radiative and convective heat transfer. In this regard, graphs were generated considering combinations of ε_h and ε_c in an attempt to find patterns which could show this influence. Since there are two walls, surfaces graphs were used to obtain a better view of these cases. The results given in Figure 10 were obtained for $Ra = 10^5$, A=1, 4, 6 and 8, $\varepsilon_{t\&b} = 0.5$.

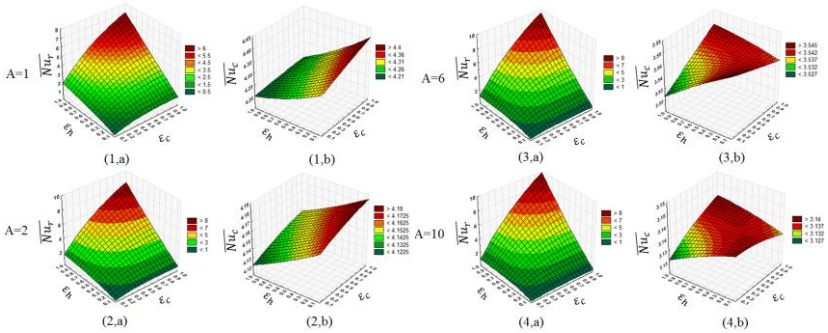

Figure 10: Surfaces showing the influence of ε_h and ε_h simultaneously. ε_t and $\varepsilon_b = 0.5$, $Ra = 10^5$.

the effect of natural convection in an enclosure without surface thermal radiation was studied. Similarly to other researchers [0,0], it can be seen in Figure 5 that in general $\overline{Nu_c}$ decreases as A increases. Nevertheless, for Ra $= 10^3$ $\overline{Nu_c}$ is almost independent of A, due to the fact that there is a strong conductive regime for this Rayleigh number. As the Rayleigh number increases, the conductive component diminishes and $\overline{Nu_c}$ becomes more dependent on A.

A two-dimensional low aspect ratio rectangular enclosure was simulated using ANSYS CFX to analyze the interaction between natural convection and surface radiation. A vertical cavity filled with air was heated from the side, with horizontal adiabatic walls and emissivities varying from 0 to 1. The study covered Rayleigh numbers ranging from 10^3 to 10^6 and aspect ratios of 1 to 10.

Firstly, a grid analysis was carried out in a square cavity with Ra $= 10^6$ and wall emissivity of 1. It was shown that it is possible to reduce the computational effort by concentrating the grid close to the walls with a bias factor of around 7. The results were compared with studies available in the literature and excellent agreement was observed.

Initial analysis showed, similarly to other studies, that $\overline{Nu_c}$ decreases as the aspect ratio (A) increases for pure convection. Nevertheless, for Ra $= 10^3$ $\overline{Nu_c}$ is almost independent of A due to the fact that there is a strong conductive regime for this Rayleigh number. As the Rayleigh number increases, the conductive component decreases and $\overline{Nu_c}$ becomes more dependent on A.

When the radiation was included, as expected, an increase in the emissivity of all walls resulted in greater radiative heat exchange and, consequently, higher $\overline{Nu_r}$ values. It was interesting to note that an increase in A leads to an increase in $\overline{Nu_r}$. The opposite was observed for $\overline{Nu_c}$ in the case of pure convection. The introduction of emissivity affected $\overline{Nu_c}$ as expected and as observed by other authors. There is a drop in $\overline{Nu_c}$ for $Ra = 10^5; 10^6$ and a slight increase in $\overline{Nu_c}$ for $Ra = 10^3$. However, $\overline{Nu_t}$ increases for all Ra values. The effect of radiation is important and, in some cases, $\overline{Nu_r}$ reached a value 350% higher than $\overline{Nu_c}$. The radiation decreases the top surface temperature and increases the bottom surface temperature. This causes a modification in the fluid temperature profile at the hot and cold walls, resulting in a reduction in the average convection Nusselt number ($\overline{Nu_c}$)

A separate analysis of the top and bottom emissivities revealed a weak influence on both $\overline{Nu_c}$ and $\overline{Nu_r}$. This influence decreases with the aspect ratio because the view factor also becomes small.

The separate analysis of cold and hot wall surface emissivity shows that Nu_r increases slightly more with increasing ε_h than with increasing ε_c. Although the effect of ε_h is greater, it is clear that Nu_r is strongly dependent on both ε_h and ε_c. Thus, if the goal is to reduce the heat transfer, decreasing the emissivity of only one of the walls is effective.

5. REFERENCES

Akiyana, M., and Chong, Q. P, Numerical Analysis of Natural Convection with Surface Radiation in a Square Cavity, Numerical Heat Transfer Part A, Applications: An International Journal of Computation and Methodology, vol. 32, no. 4, 419-433, 1997

ANSYS Workbench, Release 14.1. CFX Help Manual.

B. Ramaswamy, T. C. Jue, and J.E. Akin, “Semi-implicit and Explicit Finite Element Schemes for Coupled Fluid/Thermal Problems” International Journal of Numerical Methods in Engineering. vol 34, 675-696, 1992

Bahlaoui. A, Raji. A, Hasnaoui. M, Combined effect of radiation and natural convection in a rectangular enclosure discreetly heated from one side, International Journal of Numerical Methods for heat and Fluid Flow, vol 16, No. 4, 431-450, 2006.

Balaji, C., Venkateshan, S. P., Correlations for Free Convection and Surface Radiation in a Square Cavity**,** International Journal of Heat and Fluid Flow, Vol. 15, no. 3, 249-251,1994.

C. Balaji and S. P. Venkateshan, Interaction of Surface Radiation with Free Convection in a Square Cavity, Int. J. Heat Fluid Flow, vol. 14, no.3, pp.260-267, 1993

D.A.Mayne, A.S Usmani, M. Crapper. H-Adaptive Finite Element Solution of High Rayleigh Number Thermally Driven Cavity Problem. International Journal of Numerical Methods in Heat and Fluid Flow, vol 10, 598-615,2000

Eckert, E. G., and Carlson, W. O., Natural Convection in an Air Layer Enclosed Between Two Vertical Plates With Different Temperatures, International Journal of Heat and Mass Transfer, vol. 2, no. 1–2, pp. 106–120, 1961.

ElSherbiny. S.M, Raithby. G. D, Hollands, G. T, Heat Transfer by Natural Convection Across Vertical and Inclined Air Layers, Int. J. Heat Transfer, 104, 96-102, 1982

G de Vahl Davis. Natural convection of air in a square cavity: a benchmark numerical solution. International Journal for Numerical Methods in Fluids vol 3, 249-264, 1983

G. Barakos, E. Mitsoulis, D. Assimacopoulos, Natural convection flow in a square cavity revisited: laminar and turbulent models with wall function, International Journal for Numerical Methods in Fluids 18 (1994) 695-719.

Henkes, R. A. W. M. F. F. van der Vlugt and C. J. Hoogendoorn, 'Natural convection flow in a square cavity calculated with low-Reynolds-number turbulence models,' Int. J. Heat Mass Transfer, 34, 1543-1557 (1991).

Kim, D. M., Viskanta, R., Effect of Wall Conduction and Radiation on Natural Convection in a Rectangular Cavity, Numerical Heat Transfer Part A, Vol.7, no. 4, 449-470, 1984

Lari. K, Baneshi. M, Gandjalikhan Nassab. S. A, Komiya. A, Maruyama. S. Combined heat transfer of radiation and natural convection in a square cavity containing participating gases. International Journal of Heat and Mass Transfer 54, 5087-5099, 2011

Larson, D, W., and Viskanta, R., Transient Combined Laminar Free Convection and Radiation in a Rectangular Enclosure, Journal of Fluid Mechanics, vol.78, no.1, 65-85,1976

M.T. Manzari. An explicit finite element algorithm for convective heat transfer problems. International Journal of Numerical Methods in Heat and Fluid Flow**,** vol 9, 860-877,1999.

Markatos, N, C; Percleous, K, A. Laminar and turbulent natural convection in an enclosed cavity. International Journal Heat Mass Transfer vol 27, No. 5, 755-772, 1984

Moutaouakil. El L, Zrikem. Z, Abdelbaki. A, Interaction of Surface Radiation With Laminar and Turbulent Natural Convection in Tall Vertical Cavities: Analysis and Heat Transfer Correlations, Heat Transfer Engineering, 36:17, 1472-1484, 2015

N. Massarotti, P. Nithiarasu, O.C. Zienkiewicz, Characteristic-based-split (CBS) algorithm for incompressible flow problems with heat transfer, Int. J. Numer. Meth. Heat Fluid Flow 8 (8) (1998) 969–990.

R. K. MacGregor and A. F. Emery, 'Free convection through vertical plane layers-moderate and high Prandtl number fluids,' ASME J. Heat Transfer, 391-403 (August 1969).

Raithby, G. D., and Wong, H. H., Heat Transfer by Natural Convection Across Vertical Air Layers, Numerical Heat Transfer, vol. 4, no. 4, pp. 447–457, 1981.

Shati, A. K. A. The Interaction Between Radiation and Turbulent Natural Convection in Square and Rectangular enclosures. Doctoral thesis submitted to the University of Sheffield. Department of Mechanical Engineering. The University of Sheffield, UK. 2013

Wan, D, C ; Patnaik, B , S , V. A New Benchmark Quality Solution for the Buoyancy-Driven Cavity By Discrete Singular Convolution. International Journal of Computation and Methodology, vol 40**,** Singapore, 2001**.**

Winston. R, Diaz. G, Effect of Surface Radiation on Natural Convection in Parabolic Enclosures, Numerical Heat Transfer, Part A: Applications, 53:0, 891-906, 2008.

Xàman, J, Álvarez. G, Lira. L, Estrada. C, Numerical study of heat transfer by laminar and turbulent natural convection in tall cavities of façade elements, Energy and Building, vol 37, 787-794 (2005).

Xàman, J., Hinojosa, J. Flores, J.J, and Cabanillas, R. E., Effect of the Surface Thermal Radiation on Turbulent Natural Convection in Tall Cavities of Façade Elements, International Journal of Heat Transfer and Mass Transfer, Vol, 45, no.2, 177-185, 2008

Zitzmann, T; Cook, M; Pfrommer, P. Simulation of Steady-State Natural Convection using CFD. Ninth International IBPSA Conference Montreal, Canada, 2005

6. RESPONSIBILITY NOTICE

Leandro Manes, Eduardo Larsen Güths and Saulo Güths are the only responsible authors for the printed material included in this paper.